Post-Peak Behavior of Concrete Dams Based on Nonlinear Finite Element Analyses

Article *in* Engineering Failure Analysis · September 2021

DOI: 10.1016/j.engfailanal.2021.105778

4 authors, including:

Gabriel Sas
Luleå University of Technology
100 PUBLICATIONS **609** CITATIONS

SEE PROFILE

Richard Malm
KTH Royal Institute of Technology
67 PUBLICATIONS **454** CITATIONS

SEE PROFILE

Engineering Failure Analysis 130 (2021) 105778

Contents lists available at ScienceDirect

Engineering Failure Analysis

journal homepage: www.elsevier.com/locate/engfailanal

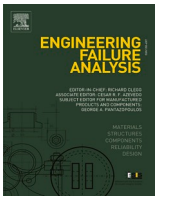

Post-peak behavior of concrete dams based on nonlinear finite element analyses

Jonas Enzell [a,*], Adrian Ulfberg [b], Gabriel Sas [c], Richard Malm [d]

[a] Dept. of Civil and Architectural Engineering, KTH Royal Institute of Technology, Brinellvägen 23, 114 28 Stockholm, Sweden
[b] Dept. of Civil, Environmental and Natural Resources Engineering, Luleå University of Technology University 97187 Luleå, Sweden
[c] SINTEF Narvik AS, Narvik 8517, Norway
[d] Dept. of Civil and Architectural Engineering, KTH Royal Institute of Technology, Brinellvägen 23, 114 28 Stockholm, Sweden

ARTICLE INFO

Keywords:
Concrete dams
Nonlinear FEM
Post-peak behavior
Displacement controlled simulations
Failure analyses

ABSTRACT

Dam failures are catastrophic events and in order to improve safety, engineers must have good tools for analysis and an understanding of the failure process. Since there are few cases of real failures in concrete dams, which can work as validation, physical model tests are a good way of improving numerical models and the understanding of the failure process. In this article, a physical model test of the buttress from a concrete Ambursen type dam is used as a benchmark for calibrating a FE-model. The dam failure is thereafter simulated using the concept of safety commonly used in the design codes. The advantages and drawbacks of performing load- and displacement-controlled simulations are compared. A new method for performing displacement-controlled simulations, using nonlinear springs to introduce the hydrostatic pressure and ice load is thereafter suggested and tested. The proposed method gives results which corresponds to the classical methods of analysis but has some advantages. Primarily, the new method is stable and does not suffer from convergence issues as was the case with the other methods. It is also simple to introduce in most commercial software compared to classical displacement-controlled simulations.

1. Introduction

In modern history, several failures in concrete dams have occurred. Most of these documented failures occurred during the early 20th century, but dam failures may still occur today. ICOLD [1] showed in their statistics of dam failures, almost half of all dam failures have occurred within the first five years after construction. Amongst these dams, the most common reason for failure is related to the initial filling of the reservoir. After this, the probability of failure has continuously been decreasing for the dams during the following 50 years of service. Their results also showed that the probability of failure increases again as the dams reach an age larger than this. This shows that aging dams are more prone to go to failure and it is likely caused by degradation mechanisms, cracking etc., that successively decrease the dam safety unless rehabilitation measure are undertaken.

It should be noted, however, that dam failures are rather uncommon compared to other types of civil engineering structures. In addition, very few, if any, dam failures are sufficiently documented to act as case studies to compare the results from numerical

* Corresponding author.
E-mail addresses: jonas.enzell@byv.kth.se (J. Enzell), adrian.ulfberg@ltu.se (A. Ulfberg), gabriel.sas@nout.no (G. Sas), richard.malm@byv.kth.se (R. Malm).

https://doi.org/10.1016/j.engfailanal.2021.105778
Received 2 April 2021; Received in revised form 22 September 2021; Accepted 24 September 2021
Available online 27 September 2021

simulations. The knowledge is therefore relatively limited regarding the failure process and post failure behavior of concrete dams.

At the time when many of the concrete dams were built, i.e. before the spread of commercial finite element software, physical model tests was the dominant method of analysis for structures with complex geometries [2]. With the development of easily accessible numerical methods, especially the finite element method, this type of analyses has nowadays taken over as the primary tool for dam safety assessments. For concrete hydraulic structures, the finite element method has successively been used to assess the safety of existing structures [3,4] or investigate the cause of cracks or their influence on the dam behavior or on the safety [5–7]. In the safety assessments, the overloading procedure is commonly used for concrete dams where the loads are increased until a failure occurs. These analyses are typically performed as load controlled where the load continuously increase in the simulation. A few cases exist where deformation-controlled analyses are performed instead, where the post-peak response is calculated with increasing displacements, see e.g. [8]. In their analyses, the purpose was to simulate cracking in a concrete gravity dam as it was subjected to overtopping.

In dam engineering, there are several cases where physical model tests have been developed and where the model of the dam is overloaded until a failure occurs and where these have been used as validation examples for numerical simulations [8–12]. In these model tests, the loading is typically achieved by applying hydraulic jacks which increase the loading until the failure occurs. In nuclear engineering, a scale test of a reactor containment building was built and loaded to failure through application of an internal hydrostatic water pressure through the use of pumps until the failure occurred, see [13]. To the authors knowledge, similar type of experiments on dams, where the dam is overtopped, and the water pressure is increased until failure cannot be found in the literature. One reason for this is naturally, that performing these types of experiments on physical scale models of dams with an open reservoir is practically difficult. However, in order to assess failure progression of dams, these types of experiments are needed in the future to be able to assess realistic failure modes. Performing displacement-controlled analyses, is one step on the way of being able to be able to assess the post-peak behavior of dam failures. Thereby, there is a need for simplified and robust methods that can be used to perform displacement-controlled analyses of dam failures.

2. Dam safety estimation procedure

2.1. Concept of safety

Concrete gravity dams consist of large cross sections and are efficiently designed to transfer the hydrostatic pressure of the reservoir to the foundation through compression. Since both concrete and rock can withstand large compressive stresses, the global safety is determined by rigid body motions and the cross-sectional design then becomes a secondary concern. Gravity dams can fail either at the interface between the dam and the rock, in the lift joints in the concrete structure, along failure planes in the rock or along crack planes in the dam body. Concrete buttress dams is one type of gravity dams, but where the thickness of the concrete members is significantly smaller. These concrete buttress dams are thereby commonly reinforced, which makes the dam act monolithically even if smaller cracks exist and thereby reduces the probability of internal failure modes. In design codes, the dam safety is normally determined by two separate global failure mechanisms, sliding and overturning [14]. The safety for overturning failure, s_{fo}, is calculated as the ratio between the overturning and the stabilizing moments, as:

$$s_{fo} = \frac{M_s}{M_d} \tag{1}$$

where M_s is the stabilizing moment and M_d is the destabilizing moment. The sliding safety, S_{fs}, is determined by the ratio of the destabilizing forces and the gravity load, if cohesion is excluded:

$$s_{fs} = tan\left(\delta_g\right)\frac{\sum V}{\sum H} \tag{2}$$

where δ_g is the friction angle in the joint or crack, $\sum H$ is the sum of the horizontal forces and $\sum V$ is the sum of the vertical forces. The factor of safety for sliding and overturning is determined in the local design codes, see e.g. USACE [14].

To determine the global dam safety for complex geometries, cracked sections or to be able to include nonlinearities, FE-simulations can be used. However, the resisting forces of a structure cannot be directly determined from a FE-simulation, the failure must therefore be simulated. A failure can be achieved in two ways, either by decreasing the strength of the material or by increasing the loads. Analogous to physical model tests, this is referred to as the reduced strength method and the overload method, respectively. When nonlinear analyses of concrete are performed, including cracking, it is not possible to reduce the material properties, since it would result in erroneous crack patterns and possibly unrealistic failure modes [15,16]. Pushover simulations are therefore usually performed when analyzing concrete dams. To achieve results corresponding to the results of the design codes, the design loads will first be applied to the dam. The driving forces are then increased by a factor λ until failure, while the resisting forces are kept constant. The factor of safety of the dam can then be calculated as the ratio between the failure load and the design load:

$$s = \frac{Failure\ load}{Design\ load} = \frac{(1+\lambda)P}{P} = 1+\lambda, \qquad \lambda > 0 \tag{3}$$

In numerical simulations, it is important to retain the resultant of each load in its original location during increased loading in order to compare with the design criterias in the codes. The reason for this is that the target safety value for global safety due to sliding and overturning is defined based on this definition. For an example, the hydrostatic pressure must increase triangularly without raising the

water level. This is analogue to raising the density of the water.

2.2. Loading algorithms for FE-simulations of failures

It is generally preferable to perform displacement-controlled loading in experiments or FE-simulations of the failure of a structure to ensure that it captures the unloading after the ultimate load [17]. In a displacement-controlled analysis, the displacement is defined at a control point, e.g. the center point of a beam. A displacement increment is applied in the control point, and remaining deformations and the loads are calculated from the equilibrium state. In a load-controlled procedure, a load increment is prescribed, and the deformation is calculated from the equilibrium. Since the load increment is predefined, the structure does not have the possibility to unload after an inflection point in the loading curve is reached. Therefore, load controlled solution algorithms can usually not be used to simulate the post-failure behavior of a structure.

The pushover analysis described in the previous section can be performed using both displacement-controlled and load-controlled solution algorithms. However, load-controlled simulations are usually used since performing displacement-controlled simulations requires subroutines in many commercial FE-software see e.g. [18–20]. During the simulated failure process of a concrete dam, the structure will reach a point of instability, after which the structure cannot sustain higher loads. After the point of instability is reached, the dam will experience large deformations due to a small incremental increase of the load. If static load-controlled simulations are performed, it will be difficult to find an equilibrium state in this stage.

To reduce convergence issues in load-controlled simulations, dynamic integration schemes can be used but this introduces kinetic forces. In these cases, a quasi-static solution is sought when using the dynamic solver. It is therefore important to ensure that the total kinetic energy in the model remain much lower than the internal energy of the model. If the load is applied too rapidly, the dynamic forces will retain the motion of the dam and it will seem that the dam can withstand higher loads, leading to unsafe estimations. Dassault Systèmes [21] recommends that the kinetic energy should remain below 5 % of the internal energy while performing quasi-static analyses. Malm [16] mentions that the total kinetic energy should be less than a few percent but that there is difficult to define an exact value.

The arc length method is a combined load- and displacement-controlled solution method, which allows for unloading [17]. It is widely used for solving buckling or other instability problems and is implemented in most commercial FE-codes. It can be used for analyzing concrete dams and might be useful when investigating global failures including the nonlinear effects from e.g. rock bolts. However, when the point of instability is reached, the structure will unload and can in some cases even provide a negative pressure to achieve force equilibrium. A drawback of the arc length method is that it is less stable than some other available options and that it suffers from convergence issues. De Borst [22] also, notes that the arch-length method is not suitable when using nonlinear material models including strain softening because the failure is highly localized.

2.3. Physical model tests

Finite element modeling has become the standard tool for analysis in the field of structural engineering because of the low cost and the limited equipment required. A good way to improve the reliability of the numerical simulations, is by validation with measured response of real cases. However, since the knowledge regarding dam failures is limited, it is difficult to find suitable validation examples. Physical scale model tests can be an effective way for calibration and validation of numerical models. Fumagalli [2] and Harris and Sabnis [23] gives examples of studies of concrete dams where physical model tests have been used for examining crack growth prediction, crack trajectory, geo-mechanical stability, and structural stability. Results from these tests can be used as benchmarks for the numerical models. Corresponding results between the two methods of analysis instills confidence in numerical models and encourages the use of numerical analyses as a complement to structural testing.

To produce a physical scale model, scaling of a real structure, the prototype, is performed. A proper scale model fulfills similitude requirements derived from dimensional analysis. The similitude requirements are based on the Pi-theorem originally described by Buckingham [24]. The theorem states that that the physical quantities are not dependent on a specific unit system and that any physical quantity can be expressed as a combination of dimensionless ratios or products of the variables that expresses the quantity. This means that two structures or systems whose dimensionless ratios and products are of the same constituents, are equivalent (i.e. similar). Therefore, a model can be created from a prototype based on the similitude requirements and be used to experimentally test the behavior of the prototype. Complete similarity between model and prototype is difficult to achieve but in order to obtain realistic results it should be met with as high accuracy as possible. However, if the examined problem is well understood and the influencing variables impact on the result is known, complete similarity may not be required as neglection of some similarity requirements could have limited impact on the investigated outcome [23].

2.4. Case study

In 2019, Sas et al. [25,26] performed physical model tests of the Norwegian Kalhovd Dam, a concrete Ambursen dam. The dam was operational in 1948 and it consists of 66 support buttresses with a height between 1.5 and 13.3 m. The dam was assessed with conventional stability analyses, see Section 2.1, where the majority of the buttresses were deemed to be unstable. It should however be noted that the actual dam showed no signs of degradation or instability. With the aim to better understand how a potential failure may occur, a buttress from the dam was reproduced in scale 1:5 and pushed to failure using hydraulic jacks, see Fig. 1. The object of the study was to investigate the influence from an irregular shape of the rock surface on the sliding and overturning stability. This was

achieved by introducing 1st order asperities at different locations along the interface between the rock and the dam. In this paper, the model tests have been used as a case study to verify the methods used for estimation of the failures of concrete gravity dams.

The original buttress was 9 m high with an inclined front plate. The physical model of the buttress wall was 1.4 m high, 0.1 m wide and made from mortar. A foundation was casted from regular strength concrete with the same width as the buttress wall. The scaled models were cast on two separate occasions where the foundation was cast first. For the casting of the buttress, the foundation was used as formwork to ensure a god fit. Cohesion between the foundation and buttress was prevented by application of rubber paint on the interface. The rubber paint was grinded off before the tests were performed to avoid reduction of the friction at the interface. The friction angle was determined experimentally using the tilt table test on concrete cube samples from each cast. The friction angle was estimated to $\phi = 30.7^{\circ}$, which corresponds to a coefficient of friction of $\mu = tan(\phi) = 0.6$.

The foundation was reinforced and made from concrete grade C30/37. The buttress was casted from a low-strength mortar mix developed specifically for the project with properties according to Table 1. The fracture energy was not experimentally tested.

The hydrostatic pressure and ice load were introduced using hydraulic jacks. The jack representing the ice load was connected directly to the upstream face of the buttress, close to the crest. The hydrostatic pressure was applied through two hydraulic jacks. These were mounted to a steel beam which distributed load from the jacks to the upstream part of the buttress. Hence, the intention of the steel beam was to ensure a load distribution that is more representative for the actual hydrostatic load. The uplift load was applied using a static weight connected to a wire and a pully system. During the experiment, the load in all hydraulic jacks were monitored. The displacements were measured using LVDT-sensors and by photogrammetry. The strains were also assessed based on the displacements obtained from photogrammetry.

3. Numerical models

The physical model tests presented in the previous section have been used as a case study to validate the numerical models and to investigate methodologies for simulating dam failures with numerical analyses. Two studies have been performed. In the first case study, the physical model test is reproduced. In the second case study, the failure of the buttress is simulated according to the concept of safety defined in the Swedish Hydropower companies guidelines for dam safety [27]. The failure is simulated using one load-controlled and one classical displacement-controlled pushover analysis. A new procedure for performing displacement-controlled pushover analyses for concrete dams, using nonlinear springs to introduce the load, is thereafter proposed, and investigated.

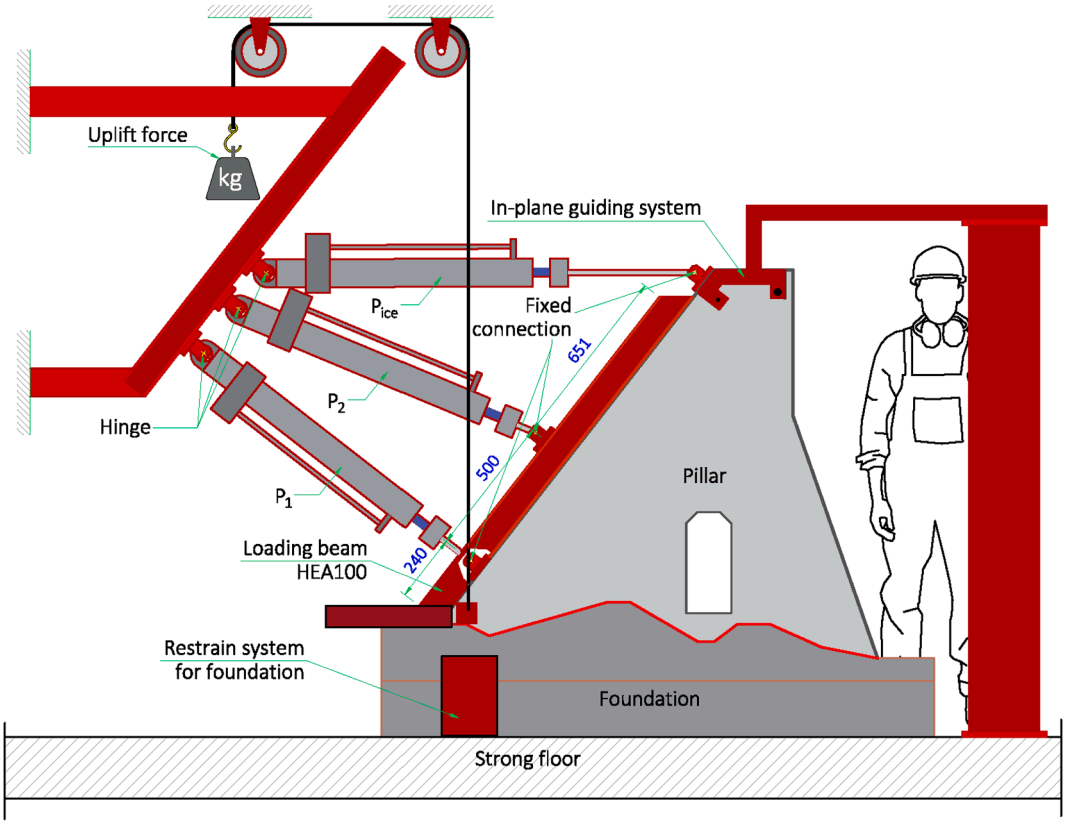

Fig. 1. Experimental setup for the physical model test performed in scale 1:5.

Table 1
Material properties for the model of the foundation and buttress wall.

Property		Buttress	Foundation
Density [kg/m]	ρ	1545	2354
Youngs modulus [GPa]	E	10.1	41.2
Tensile Strength [MPa]	f_t	0.8	
Compressive strength [MPa]	f_c	10.0	
Strain at f_c [‰]	ε_{c1}	2.5	

3.1. Geometrical model and mesh

The same geometrical model was used for all case studies. All cases were simulated using Abaqus ver. 2019 except the classical displacement-controlled simulation that was performed in Comsol Multiphysics 5.5. Comsol was used since it is easy to edit the constitutive equations and to define a displacement-controlled analyses with an arbitrary control point. The plane stress model consisted of two parts, the concrete foundation and the buttress wall. The geometry of the dam and the mesh is presented in Fig. 2. Linear, 2D plane stress elements were used, denoted CPS3 in Abaqus and Free Triangular in Comsol. The model consisted av 3564 elements and 6626 DOF. The steel beam along the front plate was defined using 75 linear beam elements, denoted B21 in Abaqus.

3.2. Material properties

In the numerical model, the foundation was modelled as linear elastic since no cracking was detected during the physical model test and the failure occurred in the buttress. The foundation was defined with material properties according to Table 1. A Poisson's ratio of $\nu = 0.2$ was assumed.

Separate simulations were performed with both linear elastic and nonlinear material properties for the buttress. The nonlinear material in the buttress was modeled using coupled damage and plasticity theory [28,29]. The initial stiffness and density for the nonlinear material models as well as the linear elastic material model were defined according to Table 1. A Poisson's ratio of $\nu = 0.2$ was assumed. The compressive behavior was modelled using the curve given for the uniaxial nonlinear behavior in Eurocode 2 [30], see Fig. 3a.

An exponential crack opening curve was used for the plastic part of the tensile behavior as defined by Reinhardt et al. [31], see Malm [32] for more information. The exponential curve is defined as:

$$\frac{\sigma}{f_t} = f(w) - \frac{w}{w_c} f(w_c) \tag{4}$$

Where $f(w)$ is a displacement function defined by:

$$f(w) = \left(1 + \left(\frac{c_1 w}{w_c}\right)^3\right) e^{-\frac{c_2 w}{w_c}} \tag{5}$$

w is the crack displacement, w_c is the stress-free crack width and $c_1 = 3.0$ and $c_2 = 6.93$ for normal strength concrete. The stress-free crack width is determined by $w_c = 5.14 G_f / f_t$ for normal strength concrete, where G_f is the fracture energy and f_t is the tensile strength.

The fracture energy will impact on the cracking behavior of concrete [6,33]. The fracture energy was not tested during the physical model tests. The buttress used in the physical model tests was created from a low-strength mortar with a short curing time. The

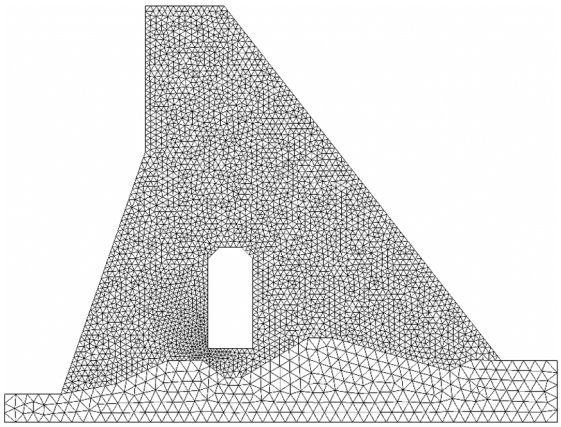

Fig. 2. Geometry and mesh of the FE-model.

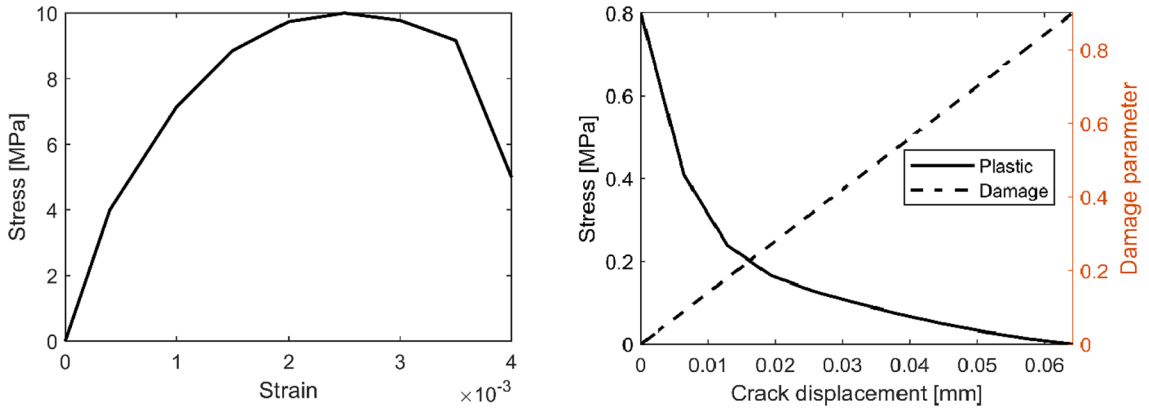

Fig. 3. a) Uniaxial plastic compressive behavior, b) crack opening curve and development of the damage parameter used for the coupled damage plasticity.

maximum aggregate size was 4 mm. This should result in a low fracture energy. Schneemayer et al. [34] tested a mortar with similar tensile strength, which has a fracture energy of 14.5 N/m. In the article, the fracture energy varies between 0.5 N/m and 63 N/m for the tested mortars although the mortar with the lowest strength was lime-based. This range was used as the basis for a parameter study to find a reasonable value for the fracture energy. The numerical model of the sliding test was used and 6 values between 5 N/m and 60 N/m were tested. The failure curves from the parameter study have been presented in Fig. 10.

The failure load decreased with decreasing fracture energy. When a fracture energy of 10 N/m and below was used, the failure mode changed where a crack appeared between the two hydraulic jacks used for applying the hydrostatic pressure. This was the same failure mode as achieved in the physical model test. A fracture energy of 10 N/m was therefore used for all subsequent analyses based on non-linear material behaviour. The uniaxial stress-displacement curve and evolution of the damage parameter used in the concrete damaged plasticity model in Abaqus is presented in Fig. 3b.

The tensile damage parameter was assumed to increase linearly from $D_t = 0$ at the onset of cracking to $D_t = 0.90$ at the crack width w_c, see Fig. 3b. When the damage parameter increases linearly, the crack opening behavior is determined by the plastic failure curve. Since the cracking was of primary interest, no compressive damage parameter was defined, i.e. the compressive failure was entirely determined by plasticity.

For defining the concrete, a dilation angle of 35° was assumed. The remaining parameters in the material model were assigned default values for concrete according to Dassault Systèmes [21], see Malm [32] for further information.

3.3. Boundary conditions and interaction

Boundary conditions were applied at the base of the foundation, preventing displacements in both directions, see Fig. 4. The buttress was connected to the foundation using an interaction. The interaction was defined to transmit compressive forces in its normal direction while not being able to carry tensile forces, i.e. resulting in joint opening. Coulomb friction, with a coefficient of friction equal

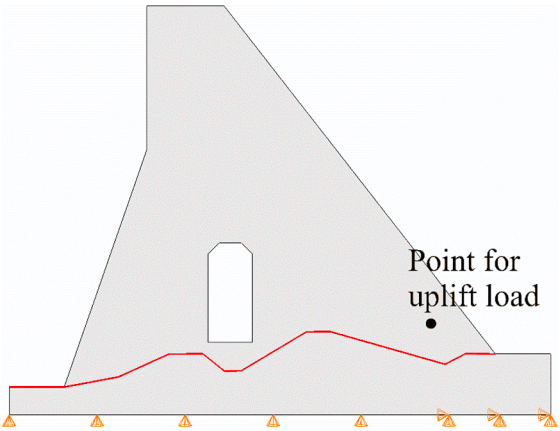

Fig. 4. Boundary conditions used in simulations and surface for interaction between dam and foundation (marked with red). The location for the uplift point load is also presented. (For interpretation of the references to colour in this figure legend, the reader is referred to the web version of this article.)

to $\mu = 0.6$, i.e. the value obtained from the material tests as seen in Section 0, was defined in the tangential behavior.

3.4. Load conditions for simulation of physical model tests

In the first case study, the experimental results were reproduced. The steel beam was included in the model, attached to the upstream face of the buttress wall using an interaction. The hydraulic jacks were reproduced using spring elements. The two springs controlling the hydrostatic pressure were attached to the beam and the spring controlling the ice load was connected directly to the dam, see Fig. 5. Boundary conditions, preventing translations but allowing rotations, were defied at the second point of the spring elements, which represents the experimental loading rig. The spring elements were defined with axial spring properties, i.e. an axial stiffness. The two lower springs, for the jacks representing the hydrostatic pressure were given a stiffness of $750kN/m$ and the spring representing the ice load was given a stiffness of $100kN/m$. To simulate the expansion of the hydraulic jack, a force was applied, which forced the spring to expand and thereby applying a resulting force on the steel beam. The spring controlling the ice load was omitted in the simulation of the sliding failure, since it was not included in this experiment.

In the experiment, the uplift was applied as steel weights guided by a pulley-system. In the numerical simulations, this was represented by a point load at the location indicated in Fig. 4. The uplift was not introduced in the numerical simulation of the sliding failure since it was not included in the physical test.

3.5. Load conditions for classical failure simulations

In the second case study, failure simulations were performed using classical pushover analyses with both load-controlled and displacement-controlled solution algorithms. In the load-controlled simulation, the hydrostatic pressure was applied as a pressure load, linearly increasing with the distance from the reservoir surface. In the failure step, only the horizontal component of the pressure was applied, see Fig. 6a. The ice load was applied as a pressure load over a distance 100 mm down from the dam crest. The pressure decreased linearly from the surface to zero at the bottom of the pressurized area. The uplift was applied as a point load in the same position as presented in Fig. 4.

In the load-controlled simulations, the gravity load was first applied in a separate step, to ensure that frictional resistance developed before any horizontal forces were applied. The hydrostatic pressure, ice load and uplift were thereafter applied to their design level. In the third stage of the analysis, the failure was simulated. The destabilizing loads were slowly increased above their design level until a failure was induced in the dam. To reduce the dynamic effects, a long failure step was used. The loads were increased over a period of 20 s. Static solvers were used for the first two simulation steps and an implicit dynamic solver was used for the quasi-static failure step.

The displacement-controlled simulation was performed using Comsol Multiphysics 5.5. The loads were applied in two steps, a static solver was used for both steps. The gravity load and the vertical hydrostatic pressure was first applied in a separate step. In the second solution step, the horizontal hydrostatic pressure, ice load and uplift were applied. A control-point was defined in the crest of the dam. A range for the crest displacements from 0 to 100 mm with 0.5 mm as increment length was applied. The solver then solved for the displacements and load levels corresponding to the specified crest displacements.

3.6. Load conditions for displacement-controlled simulation using nonlinear springs

To achieve a displacement-controlled solution, spring elements were defined along the upstream face of the buttress wall. The spring elements were given individual stiffnesses, representing the hydrostatic pressure of the specific level multiplied with the area of the buttress connecting to the spring. The springs were restrained for displacements while allowing rotation at the connection with the buttress wall, see Fig. 6b. A boundary condition was defined at the second point of the springs (on the upstream side). To impose the hydrostatic pressure, the upstream node of all springs was translated in the horizontal direction towards the dam. The ice load was applied in the same manner using a separate spring. In Table 2, the spring stiffnesses used in the simulations are presented. The spring stiffnesses are defined to give the design load when the spring is compressed 10 mm.

The buttress fails in a combined overturning and sliding failure. This means that the horizontal displacement is larger in the crest

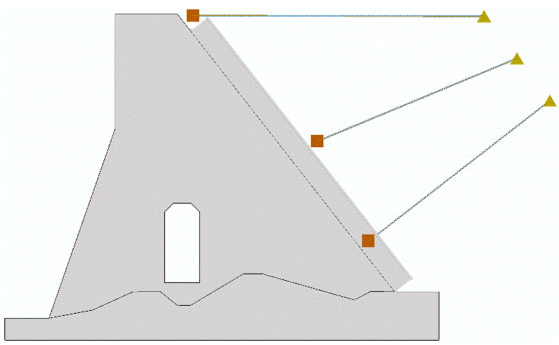

Fig. 5. Spring elements and the beam used to replicate the physical model test.

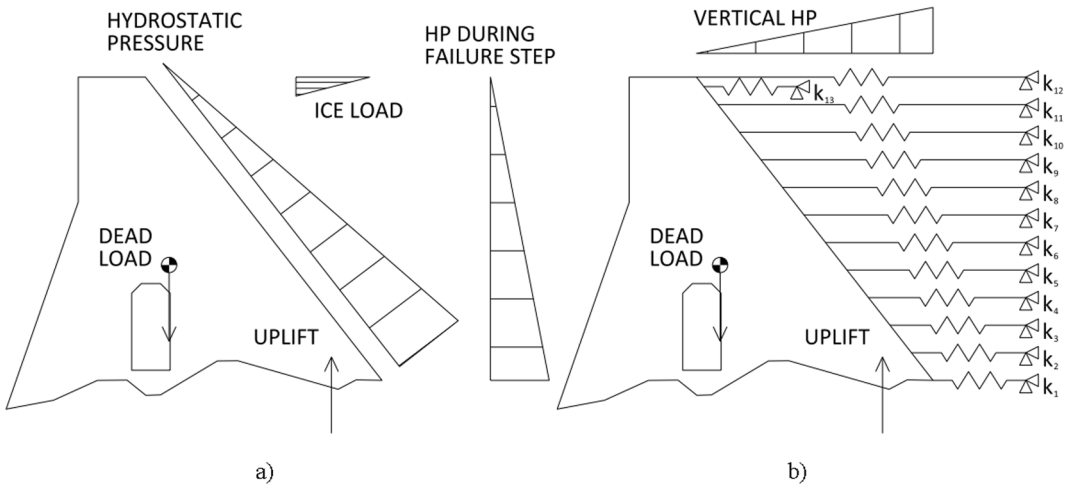

Fig. 6. a) Loads used in the load-controlled and the classical displacement-controlled simulations and b) nonlinear spring elements loads used in the suggested method for displacement-controlled simulations.

Table 2
Spring stiffnesses, k [kN/m] used in the displacement-controlled simulations.

Spring	Stiffness	Spring	Stiffness
k_1	70	k_8	51
k_2	127	k_9	38
k_3	114	k_{10}	25
k_4	101	k_{11}	13
k_5	89	k_{12}	1
k_6	76	k_{13}	170
k_7	63		

than the heel of the dam. This leads to a larger compression of the springs in the lower region of the buttress. In order to achieve a linear hydrostatic pressure during the failure, nonlinear springs with a cut-off value was used. The cut-off values were determined through an iterative procedure, where the simulation was first performed with linear elastic springs to determine the load level at failure initiation. This load level was thereafter used as the cut-off value for the final simulation with the non-linear springs. The load level in each spring was able to decrease after the cut-off was reached but not increase over that level.

The loads were applied in the same order as the load-controlled pushover simulation with the gravity load in a separate initial step. The design loads were thereafter applied, and the failure was simulated in the third and final step. Static solvers were used for the first

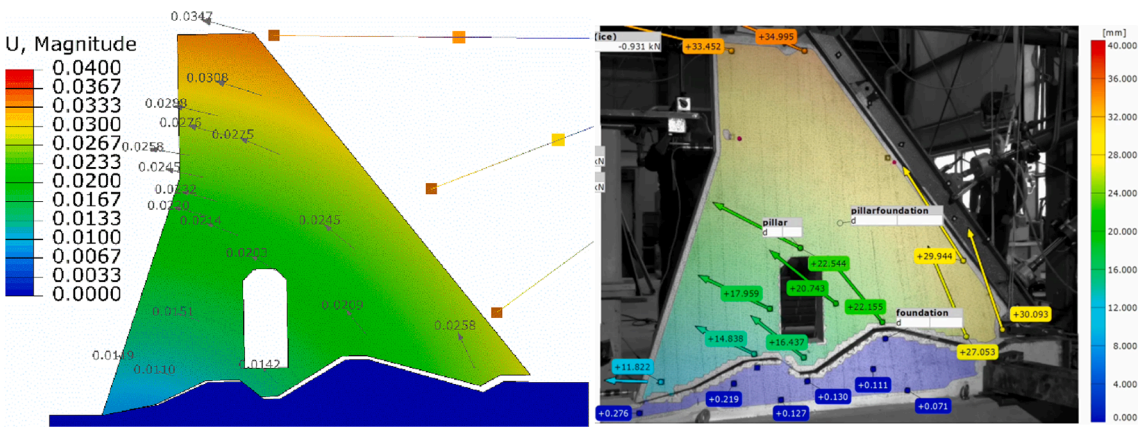

Fig. 7. Comparison between displacements in the numerical simulations and the physical model test a) simulations, unit: m b) physical model test, unit: mm.

two simulation steps and an implicit dynamic solver with a total step time of 10 s was used for the failure step.

It is not obvious how to apply the uplift pressure using the described method. The uplift should ideally be proportional to the applied hydrostatic pressure this is however difficult to achieve automatically. Instead, the uplift was iterated along with the cut-off of the nonlinear springs. The uplift was increased linearly while the hydrostatic pressure increased. Thereafter, when the cut-off value was reached for the nonlinear springs, the uplift was kept constant.

4. Reconstruction of physical model tests

In order to verify the validity of the simulations, the physical model test from Sas et al. [25] was reproduced using FE-simulations. In Fig. 7, the displacements from the numerical simulations are compared to the overturning model test. The calculated displacements correspond well with the displacements measured of the buttress. However, the displacements in the lower part of the buttress are slightly lower according to the simulation compared to the experiment. This is probably an effect of that the foundation was mounted on top of gypsum boards which were crushed during the experiments. The layer of gypsum boards was softer than the concrete used for the foundation and may thereby resulted in some displacement.

During the physical overturning model test, no cracking was reported. During the numerical simulation, some limited micro cracking occurred between the lower downstream corner of the inspection gallery and the foundation, but no macro cracks appeared.

In Fig. 8, the force–displacement graph is presented for the total force in the hydraulic jacks and the crest displacement of the dam during the overturning model test and the corresponding numerical simulations. The overturning model test was performed with two separate physical models with identical geometry and material properties. Both of the experimentally obtained curves are presented in the figure. As it can be seen in the figure, in the second test the structure was unloaded soon after the maximum load was reached since the post failure behavior was not of primary interest during the physical test. The obtained overturning failure in the experiments was accurately reproduced in the numerical simulations, where the results are in close agreement.

In Fig. 9, the resulting failure mode for the physical model test aiming to achieve a sliding failure is shown along with the corresponding failure mode obtained in the numerical simulations. As can be seen in the figure, the experiments resulted in an internal failure mode of the buttress were an inclined crack propagated from the upstream asperity towards the upstream face of the buttress. The figure also shows that the same type of failure mode and similar crack pattern occurred in the numerical simulation. However, in the numerical analyses some additional cracking appears near the inspection gallery. In the experiment, some cracking was indicated between the lower downstream corner of the inspection gallery and the foundation by the photogrammetry. It is possible that the photogrammetry does not have sufficient resolution to detect the full extent of the cracking and no crack mapping of this area was performed after the physical tests.

In Fig. 10, the failure curves from the sliding model test and the corresponding numerical simulation are presented. The buttress in the model test show a nonlinear behavior up to the failure. The final failure is brittle and occur at a load of 38*kN*. In the numerical simulation the buttress acts nonlinearly but has a slightly higher stiffness. The failure is brittle in the numerical simulation as well and occur at a total load of 42*kN*. This is 11 % higher than in the model test. Considering that this failure mode is governed by material failure, it is considered likely that repetitions of the experiment could result in scatter of this magnitude due to variations in material properties etc. It was thereby not considered to be a priority to adjust any material properties to obtain an even better fit between the experiments and the numerical analyses. Numerical analyses with lower fracture energy was however tested, but as mentioned previously, these resulted in significant convergence issues.

In Fig. 11, the tensile stress from the numerical simulations of the two failure modes are presented. In both failure modes, a crack appears between the lower downstream corner of the inspection gallery and the foundation. In the case with an overturning failure, relatively low stresses occur in the dam body and hence no additional cracking occurs during that failure mode. A stress concentration can however be clearly detected between the upper upstream corner of the inspection gallery and the upstream face of the buttress between the application point of the ice load and the upper jack controlling the hydrostatic pressure.

In the physical model tests aiming to obtain a sliding failure, the ice load was not applied and thereby stress concentrations are not expected appear in the same region. In the simulation of the sliding failure, stress concentrations appeared primarily along the

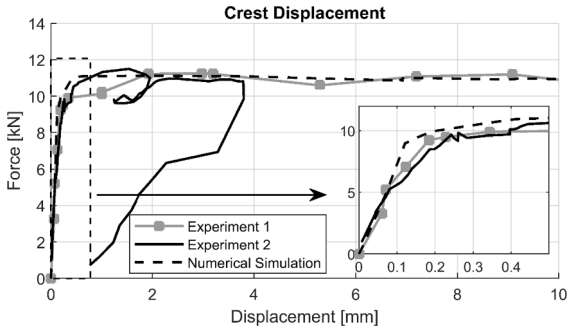

Fig. 8. Plot of crest displacements compared to the total force in the hydraulic jacks from the overturning model-test and the corresponding simulations.

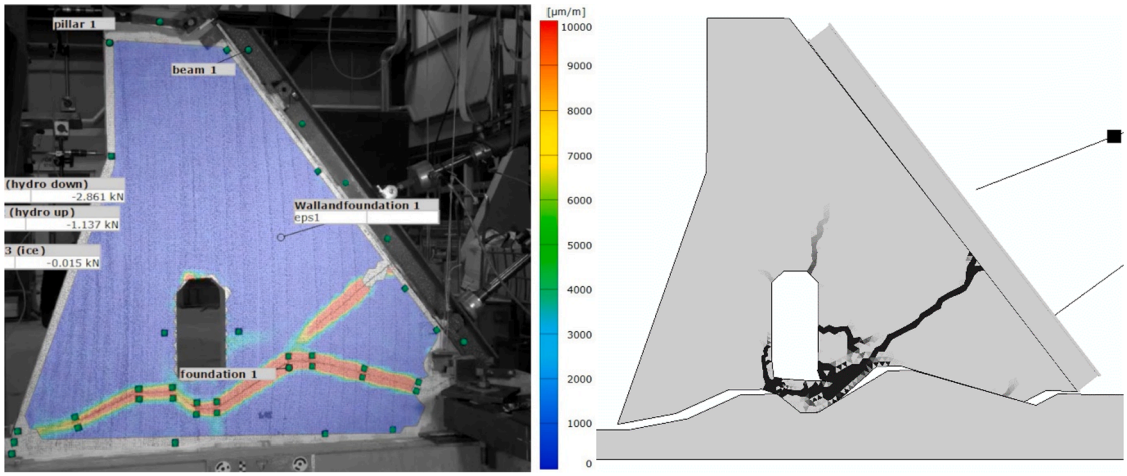

Fig. 9. Resulting failure mode during the simulation of the sliding failure for a) the physical model test and b) the numerical simulation.

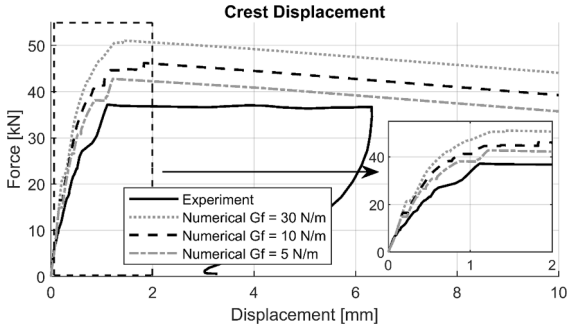

Fig. 10. Plot of force and displacements from the sliding model test compared to the corresponding simulations.

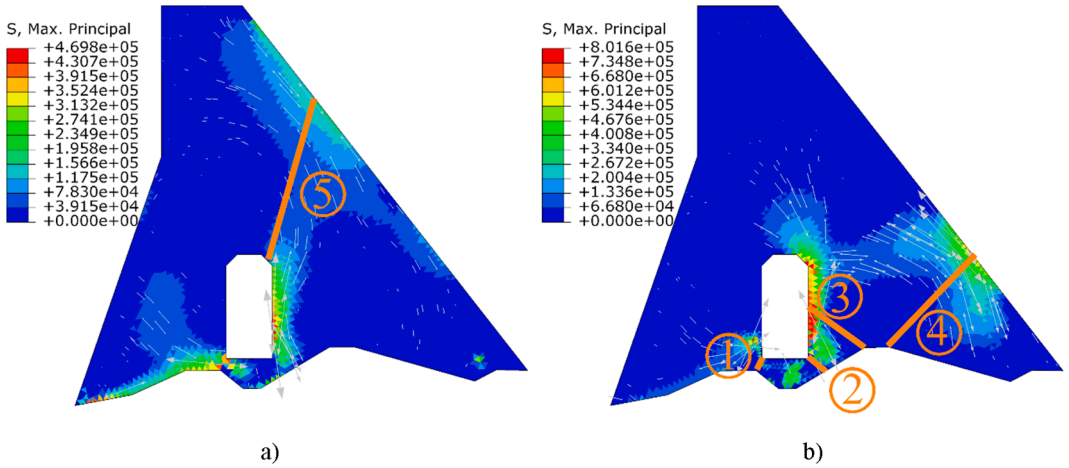

Fig. 11. Induced tensile stress in the numerical simulation of a) the overturning failure mode and b) the sliding failure mode.

upstream face of the dam and along the upstream face of the inspection gallery. These stress concentrations have been translated to five potential types of cracks that may occur, which are illustrated in Fig. 11. As can be seen in the figures, all these regions could potentially crack depending on the material properties. If spatial variations in material properties would be introduced in the simulations it is likely that, different failure modes could appear along these crack planes.

5. Simulation of failure

During the analyses, the same failure modes were obtained for all methods of analysis. Different failure modes were, however, obtained when using linear elastic and nonlinear material properties to simulate the buttress. When linear elastic properties were used, the dam failed in a combined sliding and overturning failure mode. In Fig. 12a, the failure with linear elastic material properties is illustrated. In the simulation using nonlinear material properties, the buttress started sliding while still being intact. The initial failure is therefore induced at the same load level as for the linear elastic model. After the initial slip, the buttress is restrained from further sliding due to the angle of the downstream asperity. The post-peak behavior is therefore governed by the initiation and propagation of cracks corresponding to the cracks denoted as crack 1 and 5 in Fig. 11. These cracks initiate an internal overturning failure mode. The failure mode with nonlinear material for the load-controlled simulation is presented in Fig. 12b and the failure mode for the displacement-controlled simulation using nonlinear springs. The classical displacement-controlled simulation was only performed using linear elastic material properties.

In Fig. 13, the failure curves of a classical load-controlled and displacement-controlled simulation are compared to displacement-controlled simulations using nonlinear springs. In the load-controlled simulation, the buttress wall reaches the failure load and then starts accelerating downstream. In Fig. 14a, the kinetic energy and internal energy of the load-controlled simulation is compared to the crest displacement. The kinetic energy increases over the proposed limit of 5 % of the internal energy when the load factor reaches $1 + \lambda = 1.20$, which corresponds to a crest displacement of 3.2 mm. The results past this point of the load-controlled simulations should therefore be considered as unreliable according to the previous definition by Dassault Systèmes [21].

The load–deflection curve obtained from the classical displacement-controlled simulation is also presented in Fig. 13, the failure occurs at $1 + \lambda = 1.22$. After the failure, the load decreases slightly, indicating a ductile response. Convergence issues arise which causes the simulation to stop when a crest displacement is 15 mm. The crest displacement from the displacement-controlled simulations using nonlinear spring is also presented in Fig. 13. In this simulation, the same total load of $1 + \lambda = 1.22$ is obtained at the initial failure as in the classical displacement-controlled analysis. The load–deflection curves from the two displacement-controlled simulations correlates well as can be seen in the figure. The displacement-controlled simulations using nonlinear spring are stable and can run without convergence issues with both linear and nonlinear material properties.

In Fig. 14, the ratio between the kinetic energy and the internal energy is compared to the crest displacement based on load level. It can be seen in the figure that large kinetic energy appears in the load-controlled simulation. In the displacement-controlled simulations using nonlinear springs, the ratio between the kinetic and the internal energy remains below 1 ‰ during the entire simulation. The classical load-controlled simulation is static i.e. the kinetic energy is zero by definition.

6. Discussion

The internal and global overturning failure modes obtained during the physical model tests performed by Sas et al. [25] were ductile. The cracks did however occur suddenly due to the low fracture energy of the mortar used in the model and because the reinforcement was omitted from the model. Normally slender dam structures, such as buttresses in buttress dams, are reinforced to improve the ductility of the material. The tests do however show that the cracks can appear suddenly for small displacements in the dam body. The crack patterns achieved in Section 5 closely resembles the crack patterns found in situ in a large concrete buttress dam analyzed by Malm et al. [5,35]. The crack pattern in the buttress dam was induced by seasonal variation in the ambient temperature. The cracks appear perpendicularly to the compressive forces created by the hydrostatic pressure and many passed through the inspection gallery. This shows that the same crack patterns can occur for multiple purposes. Since the cracks can appear suddenly because of multiple causes, it is important to consider potential internal failure modes which can be caused by cracks found in situ in concrete dams. This should be part of the continuous dam safety routines but possibly considered in the design of new concrete dams as well.

The defined concept of safety is important for the results since it not only defines suitable safety margins but also governs which potential failure modes that may occur. In design, the concept of safety must be in accordance with the definitions in the local codes. This is however difficult while designing physical model tests. As seen in the tests performed by Sas et al. [25], the results showed that the introduced asperities in the interface between the rock and the buttress increased the resistance for overturning and sliding failures. However, the results do not agree with the concept of safety introduced in the Swedish or Norwegian dam safety codes. This is not necessarily an issue with the model tests, since the concept of safety defined in the dam codes represent idealized failure modes that does not appear in reality. Since dam failures are complicated and highly dynamic processes including dynamic effects from the water and failures in the rock, further research in this area is required. This research could potentially result in new concepts of safety which better resembles the reality.

In the second case study, the same buttress used in the model tests was analyzed using the concept of safety defined in the dam safety codes. Two existing methodologies were compared and a new method for performing displacement-controlled simulations was proposed. The three methods gave similar results for the ultimate safety of the buttress but had different advantages and drawbacks. The load-controlled simulations are simple to perform, and the models can be defined using any commercial FE-software. The main drawback of the load-controlled simulations is that forces introduces does not have the ability to reduce after reaching an inflection point. This means that the ultimate load of the structure can be determined. However, the post failure behavior cannot be simulated.

If static solvers are used, the load-controlled simulations can suffer from convergence issues. This is usually solved by using quasi-static analyses based on dynamic solvers. In most pushover analyses of concrete gravity dams, using a dynamic solver will lead to the dam accelerating away from the initial position after the failure load is reached. The easiest way of ensuring that the load is not

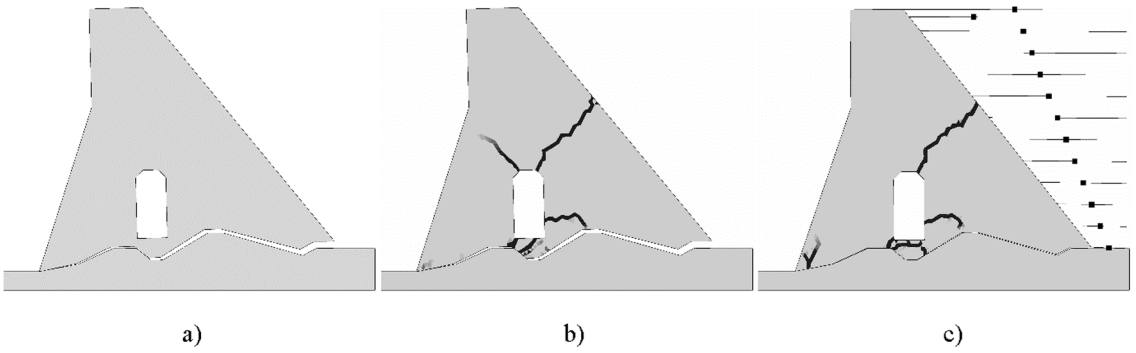

Fig. 12. Failure modes from the load-controlled simulation using a) linear elastic material properties and b) nonlinear material properties and c) displacement-controlled simulation using nonlinear material properties. The failure modes are presented for different crest displacements, Figure a and b has a crest displacement of about 50 mm and figure c has a crest displacement of 10 mm. a scale factor of 1 is used for the displacements.

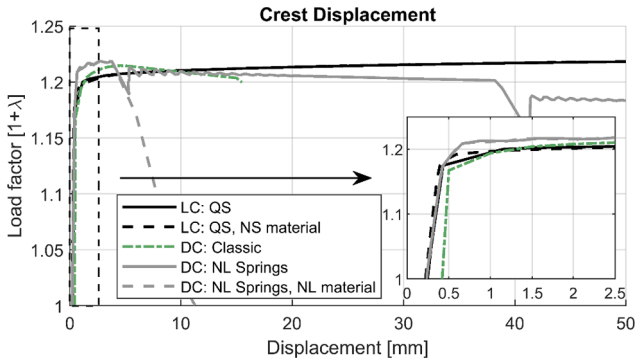

Fig. 13. Comparison between load-controlled displacement-controlled failure simulations. The curves from the two load-controlled simulations are largely overlapping and are therefore difficult to see.

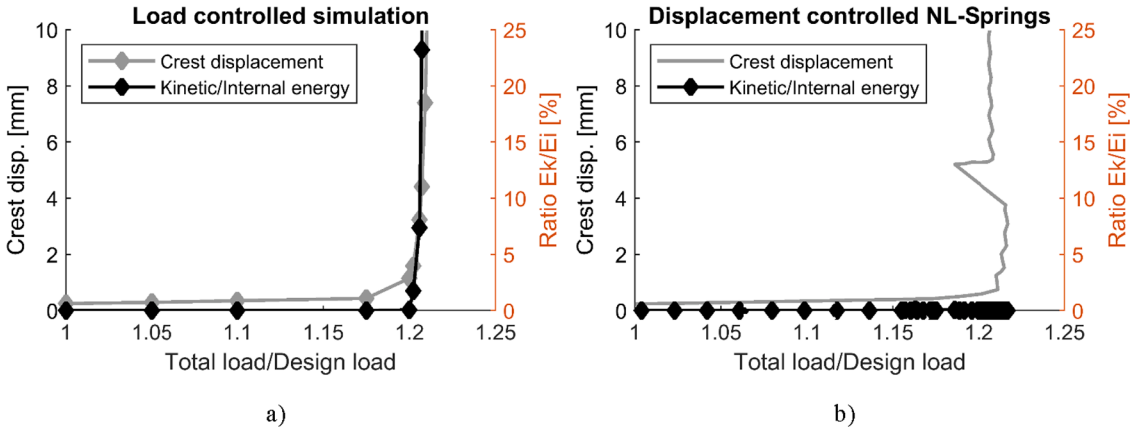

Fig. 14. Comparison between kinetic and internal energy and the relation to the crest displacement. a) Load-controlled simulation and b) displacement-controlled simulation using nonlinear springs. Both presented curves correspond to the simulations using linear elastic material properties.

overestimated is to increase the load very slowly. In this way, the dam will still accelerate away but the load will not increase higher than the failure load before the failure occurs. An analysis time of 10 or 20 s is often sufficient, but it will be up to the judgement of the engineer performing the calculations to perform a check of the reasonability of the results. It is also important to only use the load-controlled models to estimate the initial failure in the same manner as the analytical methods describes in the design codes presented in Section 2.1.

When a classical deformation-controlled simulation is performed, the loads are defined in the same manner as for the load-

controlled simulation. During the solution of an increment of the simulation, a displacement is defined, usually in the crest on a concrete dam. The remaining displacements and the loads are thereafter calculated from the equilibrium. During a displacement-controlled simulation, the load can decrease, which gives the possibility of calculating the post-failure behavior. The solution is however difficult to implement in many commercial FE-software since the constitutive equation must be altered, which may require programming of suitable routines. The simulations may also suffer from convergence issues, which can be difficult to overcome.

A new method for performing displacement-controlled simulations have been proposed. The method involves nonlinear springs which are used to introduce the hydrostatic pressure and the ice load. The method was shown to work satisfactorily on a simple geometry with nonlinear material properties. The method gives good results, which correspond with the results from the classical displacement-controlled simulations. The load has the possibility to decrease and the post failure behavior can therefore be simulated. The simulations also proved to be stable without convergence issues. The method was implemented in a quasi-static simulation. There are however some dynamics in the springs, this could be reduced somewhat by introducing a soft dashpot. The proposed method can be implemented in 2D of 3D. For 3D-structures and especially complex structures such as arch dams, the implementation could be complicated and requires a large amount of work and some programming. The way to apply uplift is not obvious while using this method. In this simple example, the uplift was applied as a point load and the amplitude varied over the failure step and was determined iteratively to match the total hydrostatic pressure. Another issue is that axial springs adds a vertical force component when the dam starts to overturn. The vertical component can however be made negligible if the axial springs are defined with a large length or nonexistent if the springs are defined to only act in in the stream direction.

7. Conclusions

Nonlinear finite element simulations are good for determining the level of safety of concrete dams with complicated geometries, existing damages or complicated loads. In addition to the classic failure modes, the simulations can capture combined failure modes and the risk for internal failure modes. The focus of this article has been to determine the post-peak behavior in order to study the ductility of the failure. This is an important part in determining the rate at which a dam failure will occur.

In the first case study, the results from physical model tests performed by Sas et al. [25] was recreated using nonlinear FE-simulations. The response of the experiments during increasing loading was successfully captured in the model and the failure modes were reproduced with good agreement. The main cracks propagated perpendicular to the compressive stress created by the hydrostatic pressure and were concentrated around the inspection gallery. The crack pattern also showed good correlation with the crack pattern typically found in situ in a large concrete buttress dam [5,35]. The concrete used in the physical model tests was brittle with a low fracture energy due to the reduced size of the experiment. The simulations showed that it is important to consider potential internal failure modes created from cracking since these may govern the dam behavior and the induced failure mode.

In this paper, two existing methods for simulating dam failures was compared and a proposed method for performing displacement-controlled simulations using nonlinear springs to introduce the loads. The results from the proposed displacement-controlled method correlated well with the results from the two existing methods. The new method allows for simulating the post failure behavior since the load can be reduced. Compared to regular displacement-controlled simulation, the new method is easier to implement in most commercial FE-software and it suffers from less convergence issues.

Declaration of Competing Interest

The authors declare that they have no known competing financial interests or personal relationships that could have appeared to influence the work reported in this paper.

Acknowledgements

The research presented was carried out as a part of Swedish Hydropower Centre - SVC. SVC has been established by the Swedish Energy Agency, Energiforsk and Svenska Kraftnät together with Luleå University of Technology, KTH Royal Institute of Technology, Chalmers University of Technology and Uppsala University. www.svc.nu.

This research has been carried out as a part of the project ‘Stable Dams’, which was funded by the Research Council of Norway (Grant No. 244029).

References

[1] ICOLD, ICOLD Incident database Bulletin 99 update -Statistical analysis of dam failures, Bulletin 188. , Committee on Dam Safety, International Commission on Large Dams (ICOLD), 2019.
[2] E. Fumagalli, Statical and geomechanical models, Springer, New York, 1973.
[3] H. Mirzabozorg, M.A. Hariri-Ardebili, M. Heshmati, S.M. Seyed-Kolbadi, Structural safety evaluation of Karun III Dam and calibration of its finite element model using instrumentation and site observation, Case Stud. Struct. Eng. 1 (2014) 6–12, https://doi.org/10.1016/j.csse.2014.02.001.
[4] R. Hellgren, R. Malm, A. Ansell, progressive failure analysis of a concrete dam anchored with passive rock bolts, Infrastructures 5 (3) (2020) 28.
[5] R. Malm, A. Ansell, Cracking of concrete buttress dam due to seasonal temperature variation, ACI Struct. J. 108 (1) (2011) 13–22.
[6] R. Malm, R. Hellgren, J. Enzell, Lessons learned regarding cracking of a concrete arch dam due to seasonal temperature variations, Infrastructures 5 (2) (2020) 19, https://doi.org/10.3390/infrastructures5020019.
[7] D. Maken, P. Léger, S.-N. Roth, Seasonal thermal cracking of concrete dams in northern regions, J. Perform. Constr. Facil 28 (4) (2013) 04014014, https://doi.org/10.1061/(ASCE)CF.1943-5509.0000483.

[8] S.S. Bhattacharjee, P. Léger, Application of NLFM models to predict cracking in concrete gravity dams, J. Struct. Eng. 120 (4) (1994) 1255–1271, https://doi.org/10.1061/(ASCE)0733-9445(1994)120:4(1255).
[9] S. Oliveiraa, R. Fariab, Numerical simulation of collapse scenarios in reduced scale tests of arch dams, Eng. Struct. 28 (10) (2006) 1430–1439, https://doi.org/10.1016/j.engstruct.2006.01.012.
[10] B. Hofstetter, G. Valentini, Review and enhancement of 3D concrete models for large-scale numerical simulations of concrete structures, Int. J. Numer. Anal. Meth. Geomech. 37 (3) (2013) 221–246, https://doi.org/10.1002/nag.1096.
[11] L. Zhang, Y.R. Liu, Q. Yang, Evaluation of reinforcement and analysis of stability of a high-arch dam based on geomechanical model testing, Rock Mech. Rock Eng. 48 (2) (2015) 803–818, https://doi.org/10.1007/s00603-014-0578-9.
[12] USBR, Investigation of the failure modes of concrete dams - Physical Model Tests, Report DSO-06-03, US Bureau of Reclamation, Denver, Colorado, 2006.
[13] M.F. Hessheimer, R.A. Dameron, Containment Integrity Research at Sandia National Laboratories – An Overview, NUREG/CR-6906, US Nuclear regulatory commission, 2006.
[14] USACE, Gravity Dam Design, Engineer Manual EM 1110-2-2200, Department of the Army, U.S. Army Corps of Engineers, Springfield, VA, USA, 1995.
[15] R. Malm, M. Könönen, C. Bernstone, M. Persson, Assessing the structural safety of cracked concrete dams subjected to harsh environment, ICOLD 2019 Annual Meeting/Symposium. Sustainable and Safe Dams Around the World, Ottawa, Canada, 2019, pp. 383-397.
[16] R. Malm, Guideline for FE Analyses of Concrete Dams. Energiforsk Report 2016:270, Energiforsk AB, Stockholm, Sweden, 2016.
[17] R. de Borst, M.A. Crisfield, J.J.C. Remmers, C.V. Verhoosel, Nonlinear Finite Element Analysis of Solids and Structures, 2nd ed., Wiley, 2012.
[18] J. Enzell, M. Tollsten, Thermal cracking of a concrete arch dam due to seasonal temperature variations, KTH Royal Institute of Technology, Stockholm, Sweden, Department of Civil and Architectural Engenering, 2017, p. 111.
[19] R. Hellgren, R. Malm, Stability assessment of concrete dams with non-linear FEA, Proceedings of the XXIII Nordic Concrete Research Symposium, Aalborg, Denmark, 2017.
[20] C. Fu, B. Hafliðason, Progressive failure analyses of concrete buttress dams: Influence of crack propagation on the structural dam safety, KTH Royal Institute of Technology, Stockholm, Sweden, Department of Civil and Architectural Engenering, 2015, p. 92.
[21] Dassault Systèmes, Abaqus 6.14 Documentation, Abaqus Analysis User's Guide [Online], 2014. http://abaqus.software.polimi.it/v6.14/. (Accessed January 25 2021).
[22] R. de Borst, Computation of post-bifurcation and post-failure behavior of strain-softening solids, Comput. Struct. 25 (2) (1987) 211–224, https://doi.org/10.1016/0045-7949(87)90144-1.
[23] H. Harris, G.M. Sabnis, Structural Modeling and Experimental Techniques (2nd ed.), CRC Press, Boca Raton, FL, USA, 1999, DOI: 10.1201/9780367802295.
[24] E. Buckingham, On Physically Similar Systems; Illustrations of the Use of Dimensional Equations, Physical Review 4(4) (1914) 345-376, DOI: 10.1103/PhysRev.4.345.
[25] G. Sas, A. Seger, D. Bista, C. Popescu, B. Arntsen, Stable Dams - Deliverable 3, Capacity and Resistance, Norut Report No.: 2019/17, Norut - Northern Research Institute, Narvik, Nowray 2021.
[26] Gabriel Sas, Cosmin Popescu, Dipen Bista, Andreas Seger, Bård Arntsen, Fredrik Johansson, Leif Lia, Influence of large-scale asperities on the shear strength of concrete-rock interface of small buttress dams, Eng. Struct. 245 (2021) 112952, https://doi.org/10.1016/j.engstruct.2021.112952.
[27] Ridas, Swedish Hydropower companies guidelines for dam safety. Application guidline 7.3 Concrete Dams (in Swedish), Svensk Energi, Stockholm, Sweden, 2017.
[28] J. Lubliner, J. Oliver, S. Oller, E. Oñate, A plastic-damage model for concrete, Int. J. Solids Struct. 25 (3) (1989) 299–326, https://doi.org/10.1016/0020-7683(89)90050-4.
[29] J. Lee, G.L. Fenves, Plastic-damage model for cyclic loading of concrete structures, J. Eng. Mech. 124 (8) (1998) 892–900, https://doi.org/10.1061/(ASCE)0733-9399(1998)124:8(892).
[30] Eurocode 2, Design of concrete structures. Part 1-1: General rules and rules for buildings SS-EN 1992-1-1:2005, Swedish Standards Institute (SIS), 2013.
[31] H.W. Reinhardt, H.A.W. Cornelissen, D.A. Hordijk, Tensile tests and failure analysis of concrete, J. Struct. Eng. 112 (11) (1986) 2462–2477, https://doi.org/10.1061/(ASCE)0733-9445(1986)112:11(2462).
[32] R. Malm, Predicting shear type crack initiation and growth in concrete with non-linear finite element method (PhD dissertation), KTH Royal Institute of Technology, Stockholm, Sweden, 2009, p. 43.
[33] A. Hariri-Ardebili Mohammad, M. Seyed-Kolbadi Seyed, H. Mirzabozorg, A smeared crack model for seismic failure analysis of concrete gravity dams considering fracture energy effects, Structural Engineering and Mechanics 48(1) (2013) 17-39, DOI: 10.12989/SEM.2013.48.1.017.
[34] A. Schneemayer, C. Schranz, A. Kolbitsch, E.K. Tschegg, Fracture-mechanical properties of mortar-to-brick interfaces, J. Mater. Civ. Eng. 26 (9) (2014) 04014060, https://doi.org/10.1061/(ASCE)MT.1943-5533.0000955.
[35] R. Malm, T. Gasch, D. Eriksson, M. Hassanzadeh, Evaluating Stability Failure Modes due to Cracks in a Concrete Buttress Dam, ICOLD 2013 International Symposium, Seattle, Washington, USA, 2013, pp. 415-424.